Magneto-optical transitions in nanoscopic rings

J. I. Climente and J. Planelles*
Departament de Ciències Experimentals, UJI, Box 224, E-12080 Castelló, Spain

W. Jaskólski
Instytut Fizyki UMK, Grudziądzka 5, 87-100 Toruń, Poland

(Received 3 March 2003; revised manuscript received 2 June 2003; published 14 August 2003)

Near-infrared spectra of self-assembled quantum rings are calculated using the $\mathbf{k}\cdot\mathbf{p}$ method with rectangular band-offset potentials in three dimensions. The effective-mass model with energy-dependent mass is employed for the electron states and the four-band Hamiltonian for the hole states. Two different ways to include the magnetic-field interaction term in the four-band Hamiltonian are compared. Our calculations describe well, qualitatively, the absorption spectrum measured by Petterson *et al.* [H. Petterson, R. J. Warburton, A. Lorke, K. Karrai, J. P. Kotthaus, J. M. Garcia, and P. M. Petroff, Physica E **6**, 510 (2000)]. and the photoluminescence magnetoresonances recently achieved by Haft *et al.* [D. Haft, C. Schulhauser, A. O. Govorov, R. J. Warburton, K. Karrai, J. M. Garcia, W. Schoenfeld, and P. M. Petroff, Physica E **13**, 165 (2002)]. The possibility of finding the ''optical'' Aharanov-Bohm effect in the state-of-the-art self-assembled InGaAs quantum rings is also discussed.

DOI: 10.1103/PhysRevB.68.075307 PACS number(s): 73.21.−b

I. INTRODUCTION

Recent advances in nanoscopic fabrication techniques have made it possible to grow self-organized InGaAs nanorings with ''volcano'' shapes.[1–7] These nanoscopic rings may be the best-suited quantum structures for investigating the electronic and optical properties of nonsimply connected quantum systems in a magnetic field,[3,8–10] as they are in the scattering-free and few-particle limit. The large body of work, both experimental[1–7,11–13] and theoretical,[8–10,14–34] which has investigated these structures since they were first synthesized,[1] reflects the great interest that the possible applications of nanoscopic quantum rings have drawn.

Whereas lots of theoretical study has been devoted to account for far-infrared electron transmission spectra in a magnetic field,[3,8,9,33,34] little effort has been made so far to provide a theoretical background to the existing experiments on interband transitions.[30] This is somewhat surprising if we consider that these transitions are the basis for the application of quantum dots as laser emitters,[35] storage devices,[36–38] fluorescence markers,[39] etc. The underlying reason may be connected with the difficulty to explain experimental data with the simple models usually employed in the literature such as the two-dimensional effective-mass model of ring with parabolic[8,9,18–25] or double-well[29,30] confining potential. In these models, the characteristic frequency of the radial confinement and the nanostructure radius are fitting parameters, and one cannot control the effects of real lateral width and inner radius of the ring, which has been proved to sensitively change the energy states of both electrons[31] and holes.[32] In the present paper, we use a truly three-dimensional model with an appropriate cylindrical square-well potential,[20] which has already described the far-infrared spectroscopy of quantum rings successfully.[33,34]

The strong nonparabolicity of the InAs conduction band[40,41] and, then, that of InGaAs, prevent the use of the parabolic band approximation, since it overestimates the electron states energy by an amount that for the studied quantum rings, is larger than the energy corrections from Coulomb interactions,[4] lattice mismatch-induced strain, and piezoelectric effects.[7] Therefore, we will employ energy-dependent mass in the Hamiltonian for electrons.

It should be finally pointed out that although single-band models have been assumed in most cases to study the hole energy levels,[16,17,19–25,28–30] in nanostructures, unlike in two-dimensional superlattices, the effects of the valence subband mixing between light hole (LH) and heavy hole (HH) are important at the Γ point.[42] By neglecting the LH-HH coupling in InGaAs, we would introduce a significant error in the estimation of the hole states energies,[43] and we would also miss allowed channels for dipole transitions. In our present calculations, we take into account the valence subband mixing by considering a four-band $\mathbf{k}\cdot\mathbf{p}$ Hamiltonian.[34,44]

We carry out calculations of the near-infrared (NIR) spectra of an InGaAs quantum ring in order to qualitatively describe the results reported by Petterson *et al.*[11] Moreover, by including a perpendicular magnetic field, we account for the experimental data reported in Ref. 12. Two different ways to insert the magnetic interaction term in the four-band Hamiltonian, namely, the traditional Luttinger approach[45] (hereafter referred to as H_L) and our recent proposal[46] (hereafter referred to as H_{ex}) are employed. We find that the calculations performed with the latter are in better agreement with the experiment. Finally, we investigate the possibility of observing the so-called ''optical'' Aharanov-Bohm effect[21–23] in the InGaAs quantum ring. Our results show no trace of this effect for the given size of the ring and low values of the magnetic field, which is also in agreement with experiment.[12]

II. THEORY

The electron states are described by means of the one-band effective-mass Hamiltonian with energy-dependent

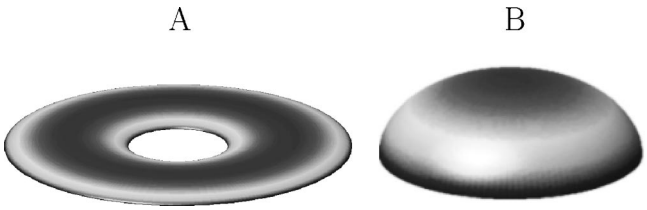

FIG. 1. Shape of the investigated quantum ring (a) and quantum lens (b). The ring height is 2 nm, the internal hole diameter 30 nm, and the external diameter 80 nm. The lens height is 6 nm and the diameter 20 nm. These shapes and sizes correspond to the nanostructures measured in Ref. 11.

(nonparabolic) mass and envelope function approximation. The corresponding equation in cylindrical coordinates, including a magnetic field perpendicular to the ring plane reads, in atomic units,

$$\left(-\frac{1}{2m^*(E_{n,m_z})}\Delta + \frac{(B\rho)^2}{8m^*(E_{n,m_z})} + \frac{Bm_z}{2m^*(E_{n,m_z})} + \frac{1}{2}\mu_B g B\sigma + V(\rho,z) - E_{n,m_z} \right) f^e_{n,m_z} = 0, \tag{1}$$

where $m_z = 0, \pm 1, \pm 2, \ldots$ is the quantum number of the projection of angular momentum $\mathbf{l}$ onto the magnetic field (B) axis, n is the main quantum number, g is the Landé factor, $V(\rho,z)$ is the quantum dot potential corresponding to the geometry shown in Fig. 1, and $m^*(E_{n,m_z})$ is the energy-dependent electron effective mass defined by[40]

$$\frac{m^*(E_{n,m_z})}{m^*(E_{n,m_z}=0)} = \frac{(E_{n,m_z}+E_g)(E_{n,m_z}+E_g+\Delta_{SO})(E_g+2\Delta_{SO}/3)}{E_g(E_g+\Delta_{SO})(E_{n,m_z}+E_g+2\Delta_{SO}/3)}, \tag{2}$$

where $m^*(E_{n,m_z}=0)$ is the electron effective mass in the vicinity of the band edge. E_g and Δ_{SO} stand for the energy band gap and spin-orbit splitting, respectively.

The valence subband mixing is taken into account by considering the two-band (actually four band with spin) $\mathbf{k}\cdot\mathbf{p}$ Hamiltonian[34,44] for the hole states. It results in a set of four coupled partial differential equations in ρ and z. In a recent paper,[46] we discussed several different ways of including the magnetic-field interaction in the multiband Hamiltonian. In the case of the four-band $\mathbf{k}\cdot\mathbf{p}$ Hamiltonian, this interaction is enclosed in the diagonal elements of the multiband equations only, so that the usual quadratic plus two linear Zeeman-like terms appear. It is not the case for the higher-number-of-bands Hamiltonians, where nondiagonal elements are also involved.[46] At the first glance, one would employ the LH and HH masses in the magnetic terms. We also pointed out in Ref. 46 that other mass coefficients may be also considered. In this paper, we show that especially good agreement with experiment is obtained when using the LH and HH masses ($1/m_{LH/HH} = \gamma_1 \pm 2\gamma_2$) in the quadratic magnetic term and an average of the HH and LH masses ($1/m_{av} = \gamma_1 - 4\gamma_2^2/\gamma_1$) in the linear terms. The corresponding Hamiltonian H_{ex} is shown in Table I. In these equations, F_z is the quantum number of the projection of the total angular momentum $\mathbf{F} = \mathbf{L} + \mathbf{J}$ onto the field axis; $\mathbf{J}$ is the Bloch angular momentum ($J = 3/2$) and $\mathbf{L}$ is the envelope angular momentum. For sake of comparison, we also employ H_L (Ref. 45) (Table 3 of Ref. 46). Equation (1) and the set of equations considered for the hole states have been solved numerically, using the finite-difference method on the two-dimensional grid (ρ,z) in cylindrical coordinates. The discretization of the differential equations yields eigenvalue problems of asymmetric huge and sparse matrices, which have been solved by the iterative Arnoldi solver[47] implemented in the ARPACK package.[48]

The electron wave function, in cylindrical coordinates, is

$$\Psi^e_{F_z} = f^e_{m_z}(\rho,z)e^{im_z\phi}|S\sigma\rangle, \tag{3}$$

where $f^e_{m_z}(\rho,z)$ is the eigenvector of Eq. (1) and $|S\sigma\rangle = |S\rangle|\sigma\rangle$ is the Bloch function for electrons, with $\sigma = \alpha$ or β.

The hole wave function reads

$$\Psi^h_{F_z} = \sum_{M_z = F_z - 3/2}^{Fz+3/2} f^h_{M_z}(\rho,z)e^{iM_z\phi}|3/2,J_z\rangle\,\delta_{J_z(F_z-M_z)}, \tag{4}$$

where $f^h_{M_z}(\rho,z)$ are the components of the four-band Hamiltonian eigenfunction and $|3/2,J_z\rangle$ are the Bloch functions for holes.

Optical transition rates between the conduction- and valence-band states are calculated without including exciton effects.[49] The optical transition matrix element, if we consider unpolarized light (i.e., we add all three x,y,z components of the transition moment) and transitions to both $|S\alpha\rangle$ and $|S\beta\rangle$ states, is just[51]

$$|\langle\Psi^e_{F'_z}|\mathbf{p}|\Psi^h_{F_z}\rangle|^2 = \left|\sum_{M_z} f^e_{m_z} f^h_{M_z}\rho d\rho dz P\right|^2 \delta_{m_z M_z} = S^2_{eh}P^2\delta_{m_z M_z}, \tag{5}$$

where S^2_{eh} is the electron-hole overlap and P is the Kane parameter, $P^2 = |\langle S|p_x|X\rangle|^2$. Note that the selection rule $\delta_{m_z M_z}$ selects, if any, only one of the four components of the hole function. In order to obtain a smooth absorption spectrum, we replace δ_{m_z,M_z} in Eq. (5) with a Lorentzian function of energy E, i.e.,

$$|\langle\Psi^e_{F'_z}|\mathbf{p}|\Psi^h_{F_z}\rangle|^2 = S^2_{eh}P^2\frac{1}{1+4\dfrac{E-E_{eh}}{\Gamma^2}}, \tag{6}$$

where E_{eh} is the e-h pair energy, $E_{eh} = E_{n',m_z} + E_g + E_{n,F_z=m_z+J_z}$ and Γ is the transition half-width.

TABLE I. Four-band $\mathbf{k}\cdot\mathbf{p}$ EFA valence Hamiltonian in cylindrical coordinates.

$\frac{(\gamma_2+\gamma_1)}{2}\left[\frac{\partial^2}{\partial\rho^2}+\frac{1}{\rho}\frac{\partial}{\partial\rho}-\frac{(F_z-1.5)^2}{\rho^2}\right]$ $+\frac{(\gamma_1-2\gamma_2)}{2}\left[\frac{\partial^2}{\partial z^2}-\frac{B^2\rho^2}{4}\right]$ $-\left(\gamma_1-\frac{4\gamma_2^2}{\gamma_1}\right)\frac{(F_z-1)B}{2}+V(\rho,z)$	$\sqrt{3}\gamma_3\left[\frac{\partial^2}{\partial\rho\partial z}+\frac{F_z-0.5}{\rho}\frac{\partial}{\partial z}\right]$	$-\sqrt{3}\frac{\gamma_2}{2}\left[\frac{\partial^2}{\partial\rho^2}+\frac{2F_z}{\rho}\frac{\partial}{\partial\rho}\right.$ $\left.+\frac{F_z(F_z-1)-0.75}{\rho^2}\right]$	0
$\sqrt{3}\gamma_3\left[\frac{\partial^2}{\partial\rho\partial z}-\frac{F_z-1.5}{\rho}\frac{\partial}{\partial z}\right]$	$\frac{(\gamma_1-\gamma_2)}{2}\left[\frac{\partial^2}{\partial\rho^2}+\frac{1}{\rho}\frac{\partial}{\partial\rho}-\frac{(F_z-0.5)^2}{\rho^2}\right]$ $+\frac{(\gamma_1+2\gamma_2)}{2}\left[\frac{\partial^2}{\partial z^2}-\frac{B^2\rho^2}{4}\right]$ $-\left(\gamma_1-\frac{4\gamma_2^2}{\gamma_1}\right)\frac{(F_z-1/3)B}{2}+V(\rho,z)$	0	$-\sqrt{3}\frac{\gamma_2}{2}\left[\frac{\partial^2}{\partial\rho^2}+\frac{2(F_z+1)}{\rho}\frac{\partial}{\partial\rho}\right.$ $\left.+\frac{F_z(F_z+1)-0.75}{\rho^2}\right]$
$-\sqrt{3}\frac{\gamma_2}{2}\left[\frac{\partial^2}{\partial\rho^2}-\frac{2(F_z-1)}{\rho}\frac{\partial}{\partial\rho}\right.$ $\left.+\frac{F_z(F_z-1)-0.75}{\rho^2}\right]$	0	$\frac{(\gamma_1-\gamma_2)}{2}\left[\frac{\partial^2}{\partial\rho^2}+\frac{1}{\rho}\frac{\partial}{\partial\rho}-\frac{(F_z+0.5)^2}{\rho^2}\right]$ $+\frac{(\gamma_1+2\gamma_2)}{2}\left[\frac{\partial^2}{\partial z^2}-\frac{B^2\rho^2}{4}\right]$ $-\left(\gamma_1-\frac{4\gamma_2^2}{\gamma_1}\right)\frac{(F_z+1/3)B}{2}+V(\rho,z)$	$-\sqrt{3}\gamma_3\left[\frac{\partial^2}{\partial\rho\partial z}+\frac{F_z+1.5}{\rho}\frac{\partial}{\partial z}\right]$
0	$-\sqrt{3}\frac{\gamma_2}{2}\left[\frac{\partial^2}{\partial\rho^2}-\frac{2F_z}{\rho}\frac{\partial}{\partial\rho}\right.$ $\left.+\frac{F_z(F_z+1)-0.75}{\rho^2}\right]$	$-\sqrt{3}\gamma_3\left[\frac{\partial^2}{\partial\rho\partial z}-\frac{F_z+0.5}{\rho}\frac{\partial}{\partial z}\right]$	$\frac{(\gamma_2+\gamma_1)}{2}\left[\frac{\partial^2}{\partial\rho^2}+\frac{1}{\rho}\frac{\partial}{\partial\rho}-\frac{(F_z+1.5)^2}{\rho^2}\right]$ $+\frac{(\gamma_1-2\gamma_2)}{2}\left[\frac{\partial^2}{\partial z^2}-\frac{B^2\rho^2}{4}\right]$ $-\left(\gamma_1-\frac{4\gamma_2^2}{\gamma_1}\right)\frac{(F_z+1)B}{2}+V(\rho,z)$

III. RESULTS

A. Absorption spectrum

Although the ring morphology has been confirmed by different microscopy techniques,[1] the question about a possible shape change after the quantum rings are covered to complete the necessary layer structure deserves to be assessed.[2] Far-infrared spectra have been thoroughly evaluated and they seem to support ringlike electronic properties.[3] Recently, Petterson *et al.*[11] carried out NIR measurements of quantum rings in order to confirm the ringlike geometry. Comparison of neutral exciton energy structure of covered rings with that of lens-shaped quantum dots[11] was qualitatively consistent with the expected properties of a quantum ring (but it could still be argued that all their ring data corresponded to dots with smaller vertical dimension and larger lateral extent). We simulate their transmission spectrum in this section by calculating the *e*-*h* interband transitions of a quantum ring and a lens-shaped quantum dot.

The shape of the ring we investigate is a cut torus [see Figure 1(a)]. This geometry corresponds to that observed in the atomic force micrograph of uncapped quantum rings.[7] According to Ref. 11, an 80 nm outer diameter, a 30 nm inner diameter, and a 2 nm height have been used. We also investigate a lens-shaped quantum dot of 6 nm height and 20 nm diameter [see Figure 1(b)]. Both ring and lens are made of InGaAs embedded in a GaAs matrix. The electron band-edge effective mass employed, $m(E_{n,m_z}=0)=0.05$ (Ref. 34), is close to the average effective masses predicted for InGaAs cut-torus shaped rings[33] and lens-shaped dots.[52] The conduction-band offset is set to 0.77 eV, roughly 70% of the band-gap difference between pure InAs and GaAs.[53] For the valence band, the InGaAs Luttinger parameters are[41] $\gamma_1=11.01$, $\gamma_2=4.18$, and $\gamma_3=4.84$. The corresponding valence-band offset is 0.38 eV, and splitoff Δ_{SO}, 0.36 eV. For simplicity, the electron and hole effective masses are considered homogeneous in the entire structure. Since the InAs energy band gap is 0.42 eV and that of GaAs 1.52 eV, a reasonable value of 0.86 eV is used for the InGaAs nanostructures studied.

Figure 2 shows the calculated absorption spectrum for the quantum ring (thick solid line) and the quantum lens (dotted

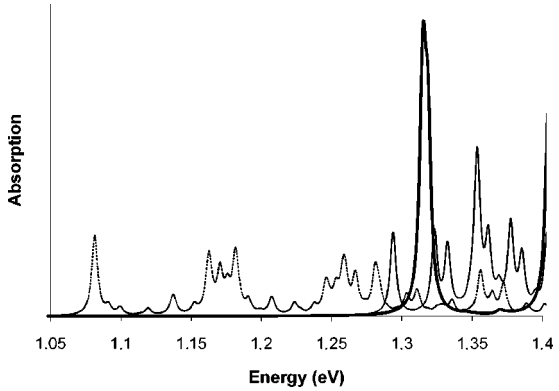

FIG. 2. Calculated absorption spectrum of an InGaAs quantum ring (thick solid line) and quantum lens (dotted line) with sizes same as those measured in Ref. 11, and absorption spectrum of a nearly flat InGaAs quantum lens (thin solid line).

line). A broadening parameter $\Gamma=5$ meV has been used to account for the size distribution in actual InGaAs self-assembled nanostructures.

For the quantum lens, the leftmost peak arises at 1.082 eV. This peak corresponds to the transition to the electron ground state $(n=1,\ m_z=0)$ from the lowest dipole-allowed hole states (all the low-lying hole states with $F_z=-1.5$, $-0.5,0.5,1.5$). As the energy increases, we observe other groups of peaks nearly evenly spaced (the energy distance between two consecutive groups being about 90 meV). Each group includes transitions from holes to a given electron state. The different groups correspond to electron states with increasing values of $|m_z|$ but the same n, i.e., transitions to $(n=1,\ m_z=0)$ appear at about 1.08 eV, $(n=1,\ |m_z|=1)$ at about 1.17 eV, $(n=1,\ |m_z|=2)$ at about 1.26 eV, etc. Transitions involving electron states with $n=2$ are usually weaker. Some of these transitions appear in the same energy region as the group of peaks corresponding to transitions to $(n=1,\ |m_z|=1)$ electron states. For example, the transitions corresponding to the $(n=2,\ m_z=0)$ electron state appear at about 1.24 eV.

In the case of the quantum ring, we only see a strong single peak at 1.314 eV. This peak originates from transitions involving the electron ground and the lowest azimuthal excited states $(n=1,\ m_z=0,\ \pm 1,\ldots)$. The first transition to the $n=2$ electron state appears at 1.406 eV. However, this peak cannot be detected in the experiment, due to the tunneling of carriers into the wetting layer produced by photons with energies beyond 1.4 eV.

The main features of our simulated spectrum agree very well with experiment (Fig. 2 of Ref. 11).

(i) In the experiment, the fundamental transition arises at 1.31 eV for rings, and slightly below 1.1 eV for lens. This is consistent with our calculated values of 1.314 eV and 1.082 eV, respectively.

(ii) In the experiment, first excited transition for the lens is about twice as intense as the fundamental transition. In our calculations, the ratio between first excited and fundamental transitions intensity is 2.2 for the lens.

(iii) In the experiment, the oscillator strength corresponding to the fundamental transition of the rings is quite stronger than that of the lens. We also predict this increment, although our estimated oscillator strength ratio of 4.5, a bit larger than the experimental value of 2.9, is close to other calculations on related systems.[28] A better fit would probably be achieved by including strain forces, *e-h* Coulomb interaction, or ring eccentricity effects, which have been proved to modify the wave function distribution.[7,24,26]

An apparent discrepancy between our calculation and the experimental data for excited states of the ring comes across. However, we should point out that recent evidences[7,12] strongly suggest that the high-energy peaks of the experimental ring spectrum do not really belong to excited-state transitions of the ring, but to the ground-state transitions of a *second type* of ring. This is most likely due to a bimodal distribution in the vertical confinement of the grown rings.[54]

In Fig. 2 we also present the calculated absorption spectrum for a lens-shaped quantum dot (thin solid line) with the same outer diameter and height as the quantum ring, namely, 2 nm height and 80.0 nm diameter. The results reveal that the oscillator strength of the fundamental transition of this lens would be far less intense than the peak which is observed in the experiment. Therefore, our model supports a ringlike morphology, discarding a simple oblate lens, as the one giving rise to the experimental data in the near infrared.

It is worth mentioning that our model, in contrast to the one used in Ref. 30, does not need to arbitrarily fit confinement ω parameter, or make assumptions on the ratio of contributions from the HH and LH states in order to correctly describe the ring energy structure. It should be additionally stressed that the parameter fitting carried out in Ref. 30 assumed that the rightmost peaks of the ring spectrum originate from transitions to excited states, an assignment no longer believed.[7,12]

B. Magnetophotoluminescence spectrum

The switch on of a magnetic field perpendicular to the growth plane of the quantum rings is of special interest because the diamagnetic properties of *e-h* pairs confined in such a topology are expected to lead to Aharanov-Bohm (AB) effects. However, there is still some uncertainty on the possibility of observing these AB phenomena in quantum ring excitons.[10,15–17,25,29] Recently, Haft *et al.*[12] measured the photoluminescence emission of quantum ring neutral excitons as a function of the applied magnetic field. We simulate this experimental spectrum using the same ring parameters as in the previous calculations. The Landé factor we employ is the estimated average for the lowest state of a cut torus, with sizes similar to that we investigate,[55] when no magnetic field is applied, $g=-3.94$.[33] Such a value of the Landé factor yields very small Zeeman spin splitting. Then, we do not need further refinements on the Landé factor description to qualitatively reproduce experimental data. For the valence-band hole states calculations, we use the above-mentioned Hamiltonians H_{ex} (Table I) and H_L (Table 3 of Ref. 46). The resulting *e-h* pair energies are shown in Figs. 3(a) and 3(b), respectively. It comes from Fig. 3 that H_{ex} describes the experiment (Fig. 1 of Ref. 12) better than H_L. Thus, H_{ex} yields diamagnetic behavior for the *e-h* pair states in agree-

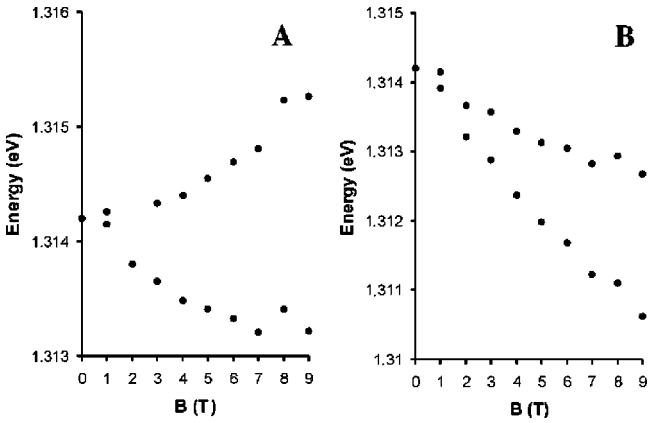

FIG. 3. Calculated photoluminescence (PL) emission spectra of a quantum ring vs a perpendicular magnetic field. (a) PL spectrum obtained with H_{ex}. (b) PL spectrum obtained with H_L.

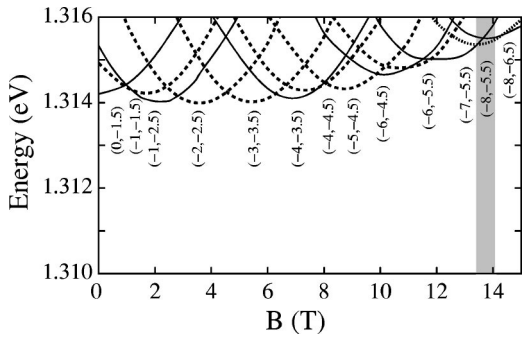

FIG. 4. Energy spectrum of the lowest-lying e-h pairs vs magnetic field. Only the states which become fundamental for some value of the field are represented. The states are labeled by (m_z, F_z). Solid lines correspond to states involving heavy hole components of the hole function. Dashed lines correspond to transitions involving light hole components. The dotted line corresponds to a ''dark'' ground state. The magnetic-field interval for which this one is the ground state is grey shaded.

ment with the experiment, which is not the case for H_L. The latter Hamiltonian predicts a strong stabilization of the lowest-lying hole states with increasing values of the magnetic field. This is reflected in the calculated photoluminescence (PL) emission as a peak redshift, which is not observed in the experiment. In contrast, H_{ex} yields a small blue shift for the PL peak, in fairly good agreement with the experiment.[12] As a matter of fact, the measured experimental PL peak exhibits a slightly stronger diamagnetic shift than the calculated one,[56] shown in Fig. 3(a). The inclusion of e-h Coulomb interaction and other minor effects might account for this discrepancy. Nevertheless, it should be stressed that this difference in diamagnetic shifts is just several μeV/T^2. Therefore, no matter what the number of refinements we would introduce in our theoretical model, the actual inaccuracy on the experimental determination of nanostructures sizes and shapes is the accuracy limiting factor of the results.

C. Optical Aharanov-Bohm effect

Figure 3 encloses the calculated ring PL energy transitions versus magnetic field given by both H_{ex} and H_L Hamiltonians. In both cases, the slope of the calculated PL energy transitions is almost constant with the field, so that no clear evidence of AB oscillations in the PL spectrum is predicted. This is in agreement with previous theoretical studies, which also predict negligible AB effect amplitudes for the actual nanorings radii and fields.[16,25,29] However, an optical consequence of the AB oscillations has been recently pointed out.[21–23] The ''optical'' AB effect holds when the magnetic field induces successive symmetry changes in the electron and hole ground states. In general, these symmetry changes occur at a different rate for electron and hole states, due to their distinct masses and lateral separation, so that certain values of the magnetic field may lead to ground-state excitons not fulfilling the interband selection rules. This would turn into a suppression of the PL emission in certain magnetic-field windows. Unlike other AB phenomena, the optical AB effect is expected to be detectable with single-dot PL spectroscopy. The theoretical model used so far to justify the optical AB effect is a quasi-one-dimensional model with one-band approximation for the hole states.[21–23] The quasi-one-dimensional model cannot account for the electron and hole wave functions compression in ρ with increasing magnetic field,[51] which we have checked to be significant for InGaAs nanorings. Moreover, the one-band approximation for the hole states misses some of the allowed channels for dipole transitions. Therefore, we employ here a more realistic model that takes into account both ring thickness and HH-LH coupling.

We investigate the optical AB effect in a ring of the same size and defining parameters as used in the preceding sections. The electron states are calculated by means of Eq. (1) and the hole states are calculated using H_{ex}. The electron spin splitting would equally affect all the low-lying energy levels, leaving results qualitatively unaltered. Thus, the electron spin-splitting term is dropped in these calculations. Figure 4 shows the lowest-lying e-h-pair energy-levels versus the applied magnetic field. The symmetry of the states is represented by (m_z, F_z), where m_z is the azimuthal quantum number of the electron state and F_z is the z projection of the total angular momentum F of the hole. In the figure, a clear aperiodicity in the ground-state angular momenta sequence, for increasing values of the field, can be seen. For magnetic-field values below 0.9 T, the ground-state symmetry is $(0, -1.5)$. This symmetry changes into $(-1, -1.5)$ between 0.9 T and 1.5 T and then keeps on changing at irregular intervals as the magnetic field increases. We illustrate this ground-state symmetry change in Fig. 5(a), where the electron (upper part) and hole (lower part) lowest-lying energy levels are depicted for magnetic field values up to 9 T. The mass of holes, heavier than the mass of electrons, leads to magnetic-field windows, for a given ground-state symmetry, wider than those of electrons. We have also carried out calculations using H_L. They show almost no width difference between the windows of electron and hole ground states [see Fig. 5(b)]. The underlying reason is that H_L leads to anticrossings for the hole states which provide LH character to the hole

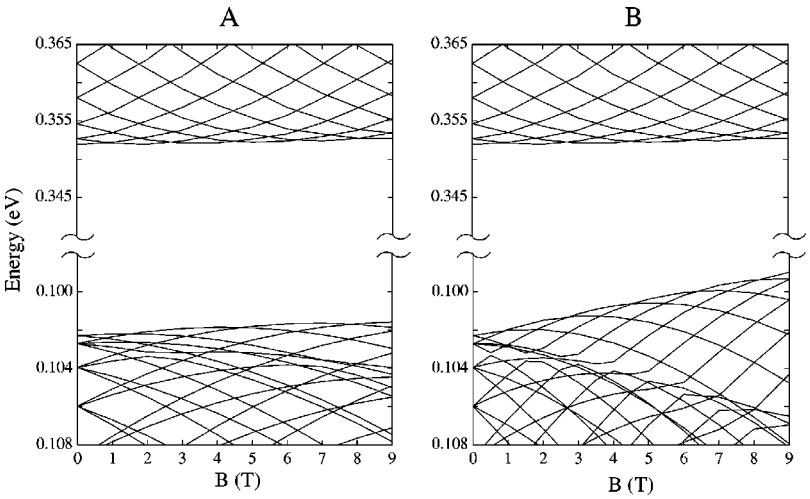

FIG. 5. Electron (upper part) and hole (lower part) energy structure vs magnetic field. H_{ex} (H_L) is used for holes in part a (b). The energy scale is referred to the bottom of the conduction band (electron) and to the top of the valence band (hole).

ground states (the mass of an InGaAs LH is 0.052, very close to the electron mass, 0.05). Conversely, H_{ex} does not yield such anticrossings and the hole ground states mainly show HH character in this case. As a consequence, Fig. 5(a) shows significant width differences between the electron and hole magnetic-field windows for a given ground-state symmetry. In what follows, we will only consider H_{ex} since it better describes the PL spectrum. The ground state in Fig. 4 occasionally involves LH components of the hole wave function (dashed lines). A simple one-band model with HH mass cannot account for these states. The suitability of a multiband Hamiltonian, which includes the HH-LH coupling, is hence confirmed.

All the *e*-*h* pairs follow, up to 9 T, the δ_{m_z,M_z} selection rule, as can be seen in Fig. 4. This is in agreement with the experiment,[12] where no magnetic-field induced quenching of the PL was detected for the same ring radii and fields as those we study here. Additionally, we explored the *e*-*h* pair ground-state symmetry for higher values of the magnetic field, looking for a trace of the optical AB effect. Our calculations reveal a dipole-forbidden (dark) *e*-*h* pair ground state, $(-8,-5.5)$, in the vicinity of 14 T (dotted line in Fig. 4). Notice that the magnetic-field window of this ''dark'' state is quite narrow (about 0.8 T) and that its energy difference with the first excited states is lower than 1 meV. The inclusion of further refinements in the theoretical model may imply a rearrangement of the energy levels and this rearrangement might, in turn, remove the dark ground state. However, the major effects we have not considered in our model are the Coulomb interaction and the strain and piezoelectric potentials. The Coulomb interaction has been theoretically proved to reduce the *e*-*h* separation.[25] In principle, this effect could shift the predicted dark ground state towards higher magnetic-field values. On the contrary, the strain and piezoelectric potentials can drastically increase the *e*-*h* vertical and lateral separation in a quantum ring.[7,13] This lateral separation would be larger than the one we estimate (barely 0.5 nm for the ground state at $B=0$ T), leading to an enhancement of the *e*-*h* symmetry change rate difference. The compensation between the Coulomb interaction and strain/piezoelectrical potentials could be partly responsible for the accuracy and reliability of our calculations, as can be seen in the PL of Fig. 3. On the other hand, the proximity between the predicted ''dark'' ground state and ''bright'' (dipole-allowed) state energies may conceal the optical AB effect due to phonon-induced energy levels coupling. However, at the temperature of experimental quantum ring PL measurements ($T=4.2$ K), these phonon-induced phenomena should not be important. We then expect that the optical AB effect could be detected in InGaAs quantum rings for relatively low magnetic fields.

IV. CONCLUDING REMARKS

We calculated near-infrared spectra of an InGaAs nanoring, modeled as a cut torus, by using the $\mathbf{k}\cdot\mathbf{p}$ method with rectangular band-offset potentials in three dimensions. For the electron states, the one-band effective mass model with energy-dependent mass and, for the hole states, a four-band Hamiltonian was employed.

We provided theoretical understanding to a number of quantum rings NIR experimental observations. First, the absorption spectrum of the quantum ring was calculated in absence of magnetic field. Two different lens-shaped quantum dots spectra were also included for comparison. Our results show excellent agreement with a recent experiment carried out by Petterson *et al.*[11] We confirm that the intense peaks they observed at high photon energies cannot be assigned to a flat quantum dot, giving then support to ringlike geometry. Second, the PL emission spectrum of the quantum ring versus perpendicular magnetic field was calculated. We compared two different ways of including the magnetic-field term in the valence-band Hamiltonian: the traditional one, reported by Luttinger[34,45] and our recent proposal.[46] We found that the latter gives better agreement with the experiment.[12] We investigated the optical AB effect[21–23] in the quantum ring. No trace of this effect was detected for magnetic-field values up to 9 T, which is in agreement with a recent experimental PL spectrum.[12] Finally, our model predicts that the optical AB effect may be seen for currently realizable quantum rings and moderate magnetic-field strenghts.

ACKNOWLEDGMENTS

We thank R. J. Warburton for helpful comments. Financial support from Generalitat Valenciana Grant No. CTIDIB-2002/189, UJI-Bancaixa Grant No. P1-B2002-01 and KBN-8T11B06218 are gratefully acknowledged. The Spanish MEC FPU grant is also acknowledged by J.I.C.

*Electronic address: planelle@exp.uji.es

[1] J.M. Garcia, G. Medeiros-Ribeiro, K. Schmidt, T. Ngo, J.L. Feng, A. Lorke, J. Kotthaus, and P.M. Petroff, Appl. Phys. Lett. **71**, 2014 (1997).

[2] A. Lorke and R.J. Luyken, Physica B **256-258**, 424 (1998).

[3] A. Lorke, R.J. Luyken, A.O. Govorov, J.P. Kotthaus, J.M. Garcia, and P.M. Petroff, Phys. Rev. Lett. **84**, 2223 (2000).

[4] R.J. Warburton, C. Schaflein, D. Haft, F. Bickel, A. Lorke, K. Karrai, J.M. Garcia, W. Schoenfeld, and P.M. Petroff, Nature (London) **405**, 926 (2000).

[5] R.J. Warburton, C. Schaflein, D. Haft, F. Bickel, A. Lorke, K. Karrai, J.M. Garcia, W. Schoenfeld, and P.M. Petroff, Physica E (Amsterdam) **9**, 124 (2001).

[6] A. Lorke, R.J. Luyken, J.M. Garcia, and P.M. Petroff, Jpn. J. Appl. Phys., Part 1 **40**, 1857 (2001).

[7] R.J. Warburton, B. Urbaszek, E.J. McGhee, C. Schulhauser, A. Hogele, K. Karrai, A.O. Govorov, J.A. Barker, B.D. Gerardot, P.M. Petroff, and J.M. Garcia, in *Physics of Semiconductors 2002*, edited by J.H. Davies and A.R. Long (Institute of Physics Conference Series, Edinburgh, 2003).

[8] A. Emperador, M. Pi, M. Barranco, and A. Lorke, Phys. Rev. B **62**, 4573 (2000).

[9] H. Hu, J.L. Zhu, and J.J. Xiong, Phys. Rev. B **62**, 16 777 (2000).

[10] J.B. Xia and S.S. Li, Phys. Rev. B **66**, 035311 (2002).

[11] H. Petterson, R.J. Warburton, A. Lorke, K. Karrai, J.P. Kotthaus, J.M. Garcia, and P.M. Petroff, Physica E (Amsterdam) **6**, 510 (2000).

[12] D. Haft, C. Schulhauser, A.O. Govorov, R.J. Warburton, K. Karrai, J.M. Garcia, W. Schoenfeld, and P.M. Petroff, Physica E (Amsterdam) **13**, 165 (2002).

[13] C. Schulhauser, D. Haft, C. Schaflein, K. Karrai, R.J. Warburton, J.M. Garcia, W. Schoenfeld, and P.M. Petroff, Physica E (Amsterdam) **13**, 161 (2002).

[14] R. Blossey, and A. Lorke, Phys. Rev. E **65**, 021603 (2002).

[15] A.V. Chaplik, Pis'ma Zh. Eksp. Teor. Fiz. **62**, 885 (1995) [JETP Lett. **62**, 900 (1995)].

[16] R.A. Romer, and M.E. Raikh, Phys. Rev. B **62**, 7045 (2000).

[17] M. Korkusinski, P. Hawrylak, and M. Bayer, Phys. Status Solidi B **234**, 273 (2002).

[18] V. Halonen, P. Pietilainen, and T. Chakraborty, Europhys. Lett. **33**, 377 (1996).

[19] H. Hu, D.J. Li, J.L. Zhu, and J.J. Xiong, J. Phys.: Condens. Matter **12**, 9145 (2000).

[20] Z. Barticevic, M. Pacheco, and A. Latge, Phys. Rev. B **62**, 6963 (2000).

[21] A.O. Govorov, A.V. Kalameitsev, R.J. Warburton, K. Karrai, and S.E. Ulloa, Physica E (Amsterdam) **13**, 297 (2002).

[22] S.E. Ulloa, A.O. Govorov, A.V. Kalameitsev, R.J. Warburton, and K. Karrai, Physica E (Amsterdam) **12**, 790 (2002).

[23] A.O. Govorov, S.E. Ulloa, K. Karrai, and R.J. Warburton, Phys. Rev. B **66**, 081309(R) (2002).

[24] I. Galbraith, F.J. Braid, and R.J. Warburton, Phys. Status Solidi A **190**, 781 (2002).

[25] J. Song and S.E. Ulloa, Phys. Rev. B **63**, 125302 (2001).

[26] L.A. Lavenere-Wanderley, A. Bruno-Alfonso, and A. Latge, J. Phys.: Condens. Matter **14**, 259 (2002).

[27] J.M. Llorens, C. Trallero-Giner, A. Garcia-Cristobal, and A. Cantarero, Phys. Rev. B **64**, 035309 (2001).

[28] B. Szafran, J. Adamowski, and S. Bednarek, J. Phys.: Condens. Matter **14**, 73 (2002).

[29] H. Hu, J.L. Zhu, D.J. Li, and J.J. Xiong, Phys. Rev. B **63**, 195307 (2001).

[30] H. Hu, G.M. Zhang, J.L. Zhu, and J.J. Xiong, Phys. Rev. B **63**, 045320 (2001).

[31] S.S. Li and J.B. Xia, J. Appl. Phys. **89**, 3434 (2001).

[32] S.S. Li and J.B. Xia, J. Appl. Phys. **91**, 3227 (2002).

[33] O. Voskoboynikov, Y. Li, H.M. Lu, C.F. Shih, and C.P. Lee, Phys. Rev. B **66**, 155306 (2002).

[34] J. Planelles, W. Jaskolski, and J.I. Aliaga, Phys. Rev. B **65**, 033306 (2002).

[35] D. Bimberg, M. Grundmann, and N.N. Ledentsov, *Quantum Dot Heterostructures* (Wiley, Chichester, 1998).

[36] G. Yusa and H. Sakaki, Appl. Phys. Lett. **70**, 345 (1997).

[37] J.J. Finley *et al.*, Appl. Phys. Lett. **73**, 2618 (1998).

[38] T. Lundstrom, W. Schoenfeld, H. Lee, and P.M. Petroff, Science **286**, 2312 (1999).

[39] M. Bruchez, M. Moronne, P. Gin, S. Weiss, and A.P. Alivisatos, Science **281**, 2013 (1998).

[40] G. Bastard, *Wave Mechanics Applied to Semiconductor Heterostructures* (Les Editions de Physique, Les Ulis, 1990).

[41] I. Vurgaftman, J.R. Meyer, and L.R. Ram-Mohan, J. Appl. Phys. **89**, 5815 (2001) and references therein.

[42] S.S. Li, J.B. Xia, Z.L. Yuan, Z.Y. Xu, W. Ge, X.R. Wang, Y. Wang, J. Wang, and L.L. Chang, Phys. Rev. B **54**, 11 575 (1996).

[43] J.B. Xia, Phys. Rev. B **40**, 8500 (1989).

[44] A. Baldereschi and N.O. Lipari, Phys. Rev. B **8**, 2697 (1973).

[45] J.M. Luttinger, Phys. Rev. **102**, 1030 (1956); M. Pacheco and Z. Barticevic, J. Phys.: Condens. Matter **11**, 1079 (1999).

[46] J. Planelles and W. Jaskolski, J. Phys.: Condens. Matter **15**, L67 (2003).

[47] W.E. Arnoldi, Q. J. Mech. Appl. Math. **9**, 17 (1951); Y. Saad, *Numerical Methods for large Scale Eigenvalue Problems* (Halsted Press, New York, 1992); R.B. Morgan, Math. Comput. **65**, 1213 (1996).

[48] R.B. Lehoucq, D.C. Sorensen, P.A. Vu, and C. Yang, ARPACK: Fortran subroutines for solving large scale eigenvalue problems, Release 2.1 (Rice University, Houston, 1995); R.B. Lehoucq, D.C. Sorensen, and C. Yang, *ARPACK User's Guide: Solution of Large-Scale Eigenvalue Problems with Implicit Restarted Arnoldi Methods* (SIAM, Philadelphia, 1998).

[49] The role of the Coulomb interaction in a quantum ring has been extensively investigated.[18,24,25] Its main effect on the lowest energy levels is a parallel shift.[18] A simple perturbation theory treatment of Coulomb interaction can successfully account for experimental data even in rings of the size we study.[4] Moreover, in InGaAs self-assembled quantum dots spectra, the effects of such a Coulomb interaction are blurred by inhomogeneous

broadening[50] and we can qualitatively describe the ring spectra without taking exciton effects into account.

[50] M. Bayer, O. Stern, P. Hawrylak, S. Fafard, and A. Forchel, Nature (London) **405**, 923 (2000).

[51] J. Climente, J. Planelles, W. Jaskolski, and J.I. Aliaga, J. Phys.: Condens. Matter **15**, 3593 (2003).

[52] B. Szafran, S. Bednarek, and J. Adamowski, Phys. Rev. B **64**, 125301 (2001).

[53] P.D. Wang, N.N. Ledentsov, C.M. Sotomayor Torres, P.S. Kop'ev, and V.M. Ustinov, Appl. Phys. Lett. **64**, 1526 (1994).

[54] H. Petterson, R.J. Warburton, A. Lorke, K. Karrai, J.P. Kotthaus, J.M. Garcia, and P.M. Petroff (private communication).

[55] The Landé factor depends only weakly on the ring parameters, and is similar for the lowest electron states in quantum rings of the size and shape we study.

[56] The better agreement of the upper branch with the experimental trends than that of the lower one might suggest that the quadratic magnetic term contribution to the energy given by our model is slightly underestimated.